J. Fluid Mech. (2010), *vol.* 661, *pp.* 32–44.
doi:10.1017/S0022112010003034

Solutions of barotropic trapped waves around seamounts

LUIS ZAVALA SANSÓN†

Department of Physical Oceanography, CICESE, Carretera Ensenada-Tijuana 3918, 22860 Ensenada, Baja California, Mexico

(Received 26 November 2009; revised 5 June 2010; accepted 5 June 2010; first published online 8 September 2010)

In this paper, solutions of free, barotropic waves around axisymmetric seamounts are derived. Even though this type of oscillation has been studied before, we revisit this problem for two main reasons: (i) the linear, barotropic, shallow-water equations with a rigid lid are now solved with no further approximations, in contrast with previous studies; (ii) the solutions are applied to a wide family of seamounts with profiles proportional to $\exp(r^s)$, with r being the radial distance from the centre of the mountain and s any positive real number. (Most previous works are restricted to the special case $s = 2$.) The resulting dispersion relation possesses a remarkable simplicity that reveals a number of wave characteristics, for instance, the discrete wave frequencies and the angular phase speed of the waves around the seamount are easily derived as a function of the seamount shape. By varying the shape parameter one can study trapped waves around flat-topped seamounts or guyots ($s > 2$) or sharp, cone-shaped topographies ($s < 2$).

Key words: shallow water flows, topographic effects, waves in rotating fluids

1. Introduction

Seamounts are abundant topographic features over the ocean floor. Nowadays there is a global estimate of more than 200 000 probable seamounts within a height range of 0.1 and 6.7 km (Hillier & Watts 2007), and this number will continue to increase as new methods and techniques of geological exploration progress. (The same authors estimate that 60 % of seamounts higher than 1 km are yet undiscovered.) The evolution of oceanic flows above and around isolated seamounts and ridges has been the subject of intensive research during the past decades. As a result, several physical mechanisms have been reported for different flow regimes: free barotropic waves (Rhines 1969), trapped waves with stratification and friction effects (Brink 1989), forced waves associated with tides (Huthnance 1974), trapped waves around non-axisymmetric seamounts (Chapman 1989), the generation of vortices (Huppert & Bryan 1976), the evolution of nonlinear vortices above seamounts (Nycander & Lacasce 2004), among many other studies where both theoretical and numerical oceanic models have been applied. A concise review of the most relevant dynamical processes over seamounts is presented in Beckman & Mohn (2002). It must also be mentioned that part of the scientific and economic interest in understanding the circulation above these topographic features is their relation with the large

† Email address for correspondence: lzavala@cicese.mx

plankton and fish abundances frequently observed above them, as widely reviewed by Genin (2004). Thus, there is strong evidence that the seamount biology is profoundly influenced by hydrodynamical processes, as pointed out by Beckman & Mohn (2002).

In this paper, we revisit the basic problem of barotropic, free waves around axisymmetric seamounts from the theoretical point of view. An approximate analytical solution for these waves was found by Rhines (1969) 40 years ago for a particular type of topography, in which the fluid depth increases proportionally to $\exp(r^2)$ from the summit of the mountain (r being the radial distance from the centre). That study showed the trapping of waves around seamounts, and that these perturbations rotate in the clockwise direction (in the Northern Hemisphere). These results have been examined under different conditions in subsequent studies. In particular, Brink (1989) numerically calculated the free modes of trapped waves around seamounts in a stratified ocean, and also devoted some attention to the barotropic case. A relevant conclusion is that waves with low azimuthal and radial wavenumbers are more likely to survive in the ocean due to resonance effects associated with tides, whilst higher wavenumber modes are damped by bottom friction. The detailed numerical simulations of Haidvogel *et al.* (1993) supported these results.

There are three main reasons for coming back to the problem of trapped waves around seamounts: (i) here, we derive new, exact analytical solutions of the barotropic problem; (ii) the solutions include a wide class of topographies, from seamounts with a very narrow summit to flat-topped seamounts or guyots; and (iii) the procedure is fairly simple and therefore widens the possibilities for attacking more complex problems on topographic waves. The existence of complete solutions reveals the exact dispersion relation of these waves with no numerical approximations. This expression shows the dependence of the wave frequency on the shape of the seamount and the angular phase speed of the waves around the topographic feature, among some other wave characteristics.

Thus, a fundamental point examined here is the shape of the mountain. For instance, several tall seamounts are characterized by a flat plateau on the summit extending a few tens of kilometres, and a pronounced steepness. Well-known structures of this type are the Great Meteor Seamount in the Atlantic Ocean (e.g. Beckman & Mohn 2002) and the Fieberling Guyot in the Pacific Ocean (see, e.g., Haidvogel *et al.* 1993). In contrast, some other seamounts have a sharp, cone-shaped summit. The solutions obtained here are a family of barotropic waves over seamounts with depth profile increasing as $\exp(r^s)$, with s being a positive real number. We first examine the case of a seamount profile with $s = 2$, considered in several other studies. Afterwards, the behaviour of trapped waves over flat-topped guyots ($s > 2$) or sharp-peak ($s < 2$) mountains is analysed.

The rest of this paper is organized as follows. The family of topographic wave solutions in the presence of an axisymmetric seamount is derived in § 2. In § 3 some examples are presented for different seamount profiles (different values of the parameter s). The discussion is presented in § 4.

2. Solutions

Using polar coordinates, the linear shallow-water equations for a homogeneous fluid layer in a rotating system are

$$u_t - fv = -g\eta_r, \tag{2.1}$$

$$v_t + fu = -\frac{g}{r}\eta_\theta, \tag{2.2}$$

$$\frac{1}{r}(rhu)_r + \frac{1}{r}(hv)_\theta = 0, \tag{2.3}$$

where subindices denote partial derivatives, u and v are the velocity components in the radial and azimuthal directions, respectively, η is the free-surface deformation, h is the fluid-layer depth, f is the Coriolis parameter (assumed constant) and g is gravity. Note that the rigid-lid approximation has been applied in the continuity equation: the fluid depth, $h(r, \theta)$, is considered time-independent. Hereafter, we consider the fluid depth associated with an axisymmetric seamount $h(r)$. From continuity, the velocity components can be defined in terms of the derivatives of a transport function $\psi(r, \theta, t)$ as

$$u = \frac{1}{hr}\psi_\theta, \quad v = -\frac{1}{h}\psi_r. \tag{2.4}$$

The vorticity equation is derived by subtracting the appropriate derivatives of the momentum equations, which yields

$$\left[\frac{1}{r}(rv)_r - \frac{1}{r}u_\theta\right]_t + f\left[\frac{1}{r}(ru)_r + \frac{1}{r}v_\theta\right] = 0. \tag{2.5}$$

This expression states that changes of relative vorticity (first term) are associated with horizontal divergence or convergence of the flow (second term) as fluid columns experience changes of depth. Substituting the divergence obtained from the continuity equation and the expressions for the velocity components (see (2.4)) gives the following equation for the transport function:

$$\psi_{rrt} + \left(\frac{1}{r} - \frac{h_r}{h}\right)\psi_{rt} + \frac{1}{r^2}\psi_{\theta\theta t} + \frac{f}{r}\frac{h_r}{h}\psi_\theta = 0. \tag{2.6}$$

Wave solutions are proposed to be of the form

$$\psi(r, \theta, t) = h(r)^{1/2}\phi(r)\exp[\mathrm{i}(\omega t + n\theta)], \tag{2.7}$$

where the azimuthal wavenumber n is a positive integer and ω is the wave frequency. This yields an equation for the radial function:

$$\phi_{rr} + \frac{1}{r}\phi_r + \left[\left(\frac{1}{2}\frac{h_r}{h}\right)_r - \left(\frac{1}{2}\frac{h_r}{h}\right)^2 + \frac{1}{2r}\frac{h_r}{h} - \frac{n^2}{r^2} + \frac{fn}{\omega r}\frac{h_r}{h}\right]\phi = 0. \tag{2.8}$$

Note that the complete radial part of solutions (2.7), $h^{1/2}\phi$, is the only one for which the surviving factor of the first derivative of ϕ is $1/r$ in (2.8), as noted by Rhines (1969) (in the context of continental shelf waves, see also Gill 1982, p. 409). Rhines (1969) derived an equivalent expression for an axisymmetric seamount with profile $h \propto \exp(r^2)$. In addition, he neglected the second term in the square bracket in order to obtain solutions in terms of Bessel functions. A different approach is followed here. First, the depth profile and its first derivative have the following form:

$$h(r) = h_0\exp(\lambda r)^s \quad \Rightarrow \quad \frac{h_r}{h} = s\lambda(\lambda r)^{s-1}, \tag{2.9}$$

where h_0 is the minimum depth at the summit, λ^{-1} is the horizontal length scale of the seamount and the parameter s measures the shape of the mountain: for small s, the mountain is very steep near the summit and less steep far from it; in contrast, for large s the summit is nearly flat whilst the topography is rather abrupt for a distance larger than λ^{-1}. Secondly, the full equation is considered with no approximations,

which yields

$$\phi_{rr} + \frac{1}{r}\phi_r + \left[\left(\frac{s^2}{2} + \frac{fns}{\omega}\right)\lambda^s r^{s-2} - \frac{s^2\lambda^{2s}}{4}r^{2s-2} - \frac{n^2}{r^2}\right]\phi = 0. \tag{2.10}$$

Now the following change of variable is applied:

$$\rho = (\lambda r)^s, \quad \chi(\rho) = \phi(r), \tag{2.11}$$

which yields the equation for the new dependent variable

$$\rho\chi_{\rho\rho} + \chi_\rho + \left(\frac{1}{2} + \frac{fn}{s\omega} - \frac{\rho}{4} - \frac{n^2}{s^2\rho}\right)\chi = 0. \tag{2.12}$$

This expression is exactly the self-adjoint form of the associated Laguerre equation (Arfken 1970, p. 620):

$$\rho\chi_{\rho\rho} + \chi_\rho + \left(\frac{2p+k+1}{2} - \frac{\rho}{4} - \frac{k^2}{4\rho}\right)\chi = 0, \tag{2.13}$$

with solutions in terms of the associated Laguerre polynomials $L_p^k(\rho)$,

$$\chi(\rho) = \exp(-\rho/2)\rho^{k/2}L_p^k(\rho), \tag{2.14}$$

where $k > -1$ is a real number and $p \geqslant 0$ is an integer. By comparing the terms inside brackets in (2.12) and (2.13), we note that these indices are given by

$$k = \frac{2n}{s}, \tag{2.15}$$

$$p = \frac{n}{s}\left(\frac{f}{\omega} - 1\right). \tag{2.16}$$

These definitions provide some important properties of the waves around the seamount:

(i) The dispersion relation of the waves is derived from the expression for p:

$$\frac{\omega}{f} = \frac{n}{sp+n}. \tag{2.17}$$

Hence, the frequency depends on integers $n \geqslant 1$, $p \geqslant 0$ and the real number $s > 0$.

(ii) The angular phase speed around the seamount is

$$c_{n,p}(s) = \frac{\omega}{n} = \frac{f}{sp+n}, \tag{2.18}$$

which shows that waves rotate around the mountain with angular speeds depending inversely on s, n and p.

(iii) If p is zero then $\omega = f$, resulting in a family of inertial motions (for different values of n and s). Besides, the fastest oscillation around the seamount is $(n, p) = (1, 0)$, which rotates around the mountain in one inertial period, $c_{1,0}(s) = f$, regardless of the shape of the mountain. However, previous studies indicate that trapped waves around seamounts are subinertial; so this analytical result should be taken with caution, as pointed out in § 4.

In order to find the complete solutions, we first note that the dimensional form of the radial function is

$$\phi(r) = A\exp(-\lambda^s r^s/2)(\lambda^s r^s)^{k/2}L_p^k(\lambda^s r^s), \tag{2.19}$$

where A is an arbitrary constant with appropriate units. When substituted in (2.7), the full solution for the transport function is

$$\psi(r,\theta,t)=\psi_0(\lambda r)^n L_p^{2n/s}(\lambda^s r^s)\exp[\mathrm{i}(\omega t+n\theta)], \tag{2.20}$$

where $\psi_0 = Ah_0^{1/2}$ is the arbitrary amplitude.

The horizontal velocity components are calculated by means of expression (2.4) and by taking the real parts:

$$u=-\frac{\psi_0 n\lambda}{h_0}\exp(-\lambda^s r^s)(\lambda r)^{n-1}L_p^{2n/s}(\lambda^s r^s)\sin(\omega t+n\theta), \tag{2.21}$$

$$\begin{aligned} v=&-\frac{\psi_0\lambda}{h_0}\exp(-\lambda^s r^s)(\lambda r)^{n-1}\\ &\times\left[(sp+2n)L_p^{2n/s-1}(\lambda^s r^s)-nL_p^{2n/s}(\lambda^s r^s)\right]\cos(\omega t+n\theta), \end{aligned} \tag{2.22}$$

where the r-derivative of the transport function is calculated by using a suitable recurrence relation of the associated Laguerre polynomials (see the Appendix). Finally, the relative vorticity field is calculated by using appropriate recurrence relations for the polynomials again:

$$\begin{aligned} \zeta=&-\frac{\psi_0\lambda^2}{h_0}\exp(-\lambda^s r^s)(\lambda r)^{n-2}\\ &\times\left[sn\lambda^s r^s L_p^{2n/s}(\lambda^s r^s)-(sp+2n)^2 L_p^{2n/s-1}(\lambda^s r^s)\right.\\ &\left.+(sp+2n)(sp+s)L_{p+1}^{2n/s-1}(\lambda^s r^s)\right]\cos(\omega t+n\theta). \end{aligned} \tag{2.23}$$

The polynomials are written in a form such that the corresponding indices are within the range of permitted values (see the Appendix for further details).

Another important point to notice is that the transport function (2.20) increases indefinitely for large r. This is a consequence of using the depth profile proportional to $\exp(r^s)$, which also diverges. However, the velocity components and the vorticity field are proportional to $\exp(-r^s)$ and therefore these fields converge for large r. From the oceanographical point of view, the physical validity of the solutions is then restricted to some finite distance proportional to the length scale of the mountain, λ^{-1}. This is further discussed in § 4.

3. Examples

In order to describe the structure and evolution of the waves, three representative cases of seamounts of the form (2.9) are presented in this section: with $s=1, 2$ and 6. The corresponding profiles are shown in figure 1. Hereafter, in all cases the minimum depth (at the origin) is $h_0 = 500$ m and the length scale of the mountain is $\lambda^{-1} = 20$ km. A Coriolis parameter of 10^{-4} s^{-1} is considered, which gives an inertial period of $T \approx 0.72$ days. Finally, recall that the wave solutions have an arbitrary amplitude determined by ψ_0, which, for simplicity, is taken as unity.

3.1. *Typical seamount profile* ($s=2$)

The seamount with shape parameter $s=2$ was considered by Rhines (1969) and has been used in several other studies (e.g. Brink 1989). In order to appreciate the azimuthal structure of waves over this feature, figure 2 shows the vorticity and velocity fields at time $t=0$ of three waves with $n=1, 2, 3$ and setting $p=1$. The vorticity field is composed of $2n$ cells with alternate signs around the seamount. Thus, for instance,

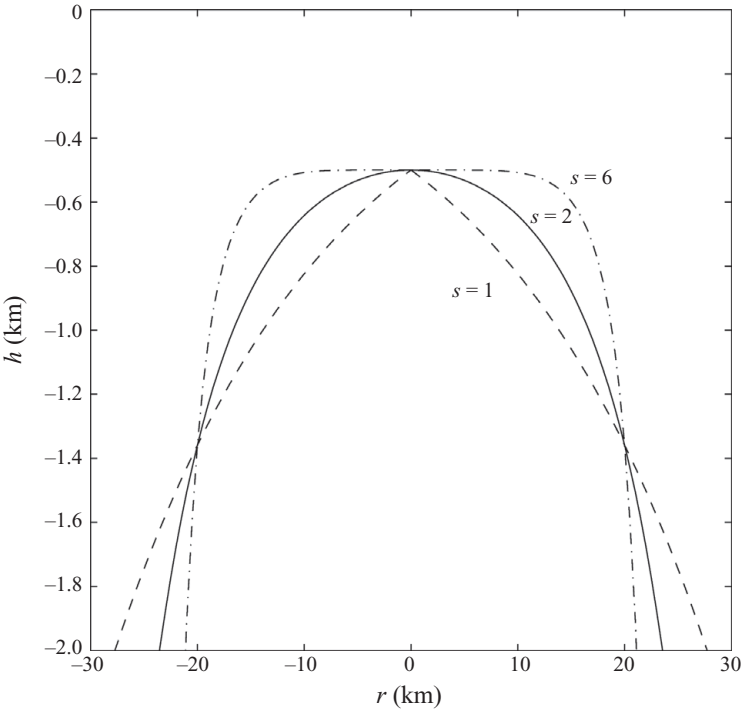

FIGURE 1. Depth profiles over seamounts of the form $h = h_0 \exp(\lambda^s r^s)$: $s = 1$ (dashed line), $s = 2$ (solid line) and $s = 6$ (dashed–dotted line). Topographic parameters are $h_0 = 500$ m and $\lambda^{-1} = 20$ km.

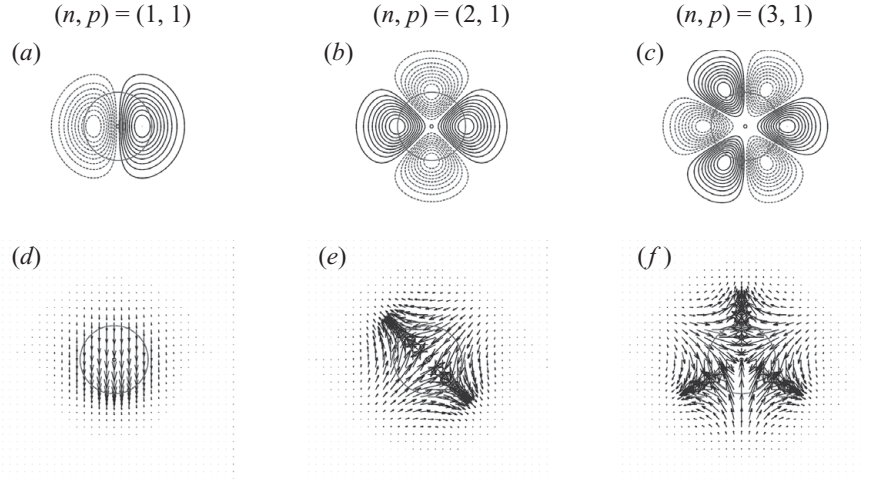

FIGURE 2. Azimuthal structure of topographic waves over a seamount with $s = 2$. (*a–c*) Relative vorticity contours for waves with azimuthal wavenumber $n = 1$, 2 and 3. In all cases $p = 1$. Continuous (dashed) contours indicate positive (negative) vorticity values of arbitrary magnitude. The contour interval is one-tenth of the maximum value. The seamount is indicated by a grey circle with radius $\lambda^{-1} = 20$ km. (*d–f*) Horizontal velocity vectors for the same waves. The magnitude of the vectors is arbitrary.

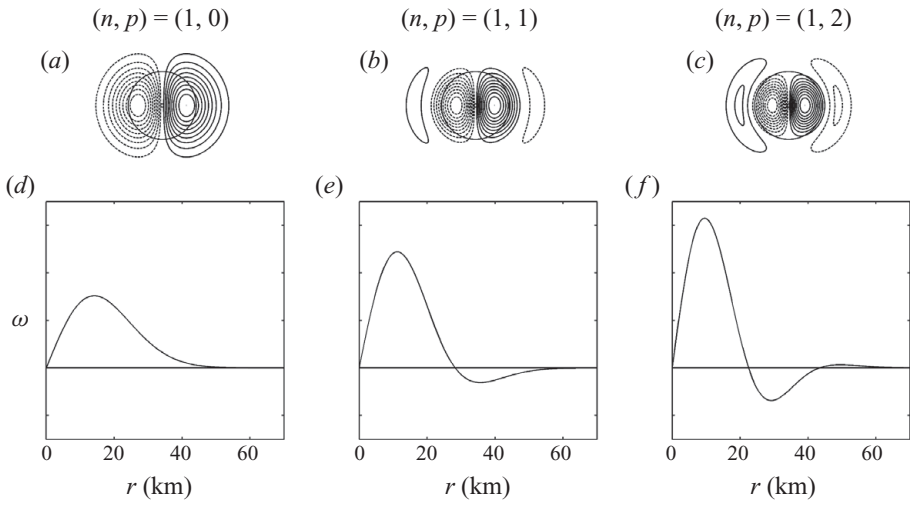

FIGURE 3. Radial structure of topographic waves over a seamount with $s = 2$. (a–c) Relative vorticity contours for waves with radial wavenumber $p = 0$, 1 and 2. In all cases $n = 1$. Contours and grey circle as in previous figure. (d–f) Radial vorticity profiles of the same waves. The profiles begin at the origin and continue along the (eastward) horizontal direction. Vorticity values on the vertical axis are arbitrary.

the case $n = 1$ shows a dipolar structure, which has been described in previous studies (Beckman & Mohn 2002). Note that these cells are arranged along the circumference with radius λ^{-1} (indicated with a black line). Accordingly, the velocity field shows an equivalent distribution of counter-rotating cells.

Figure 3 shows the radial structure of three cases with $p = 0, 1, 2$ and setting $n = 1$. Recall that index p is allowed to be zero. As mentioned above, the corresponding azimuthal distributions for $n = 1$ are dipolar modes, as shown by the corresponding vorticity fields. The radial structure is presented in figure 3(d–f), where radial profiles of the vorticity field are plotted. These profiles show an oscillatory behaviour with decreasing amplitude for large radial distances. Note that index p indicates the number of radial zero crossings of the vorticity. For $p = 0$, there are no zero crossings: the profile reaches a maximum and asymptotically approaches zero for large r. For $p = 1$, there is one zero crossing, after which the profile asymptotically approaches zero. Equivalently, for $p = 2$, there are two zero crossings. Thus, index p is a natural measure of the radial structure or, in other words, the radial wavenumber. It is also worth noticing that the amplitude of the profile rapidly decreases with r.

The dispersion relation for this seamount, $\omega/f = n/(2p + n)$, is plotted in figure 4 for different values of n and p. This plot is made in a way similar to figure 3 of Brink (1989): waves exist only at discrete points, and dashed lines are drawn just for clarity. Waves with radial wavenumbers equal to or larger than 1 ($p = 1, 2, \ldots$) show a subinertial frequency that increases with azimuthal wavenumber n; in fact, for very large n their frequency asymptotically approaches f. Another important point to consider is that waves with radial number p equal to zero correspond to oscillations with inertial frequency for any azimuthal mode n (horizontal line).

The topographic waves progress around the seamount in an anticyclonic direction. This behaviour has been described by Rhines (1969) and many others in subsequent studies. By using expression (2.18) the angular phase speed is $c_{n,p}(2) = f/(2p+n)$. For instance, for waves in figure 2 the angular phase speeds are $c_{1,1}(2) = f/3$, $c_{2,1}(2) = f/4$

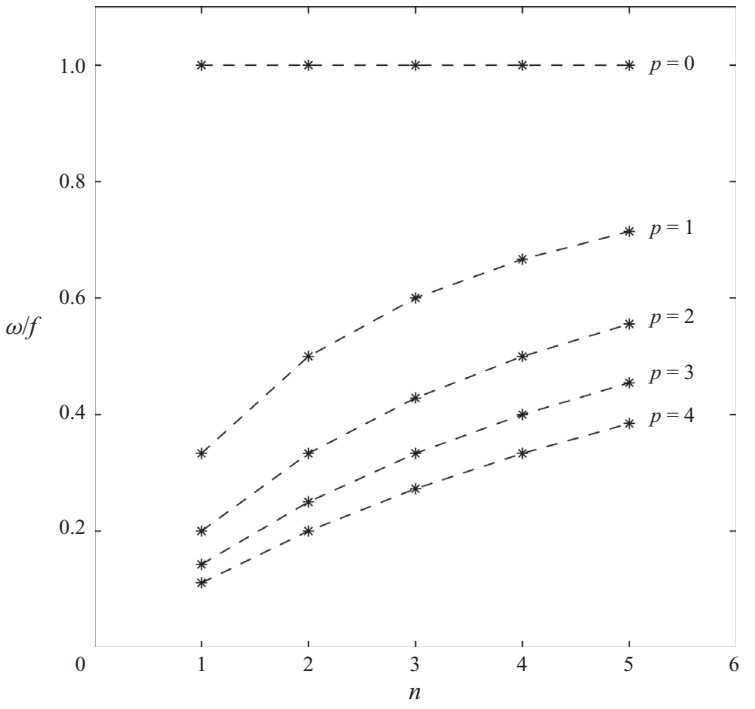

FIGURE 4. Dispersion relation for waves over a seamount with $s = 2$ (using $f = 10^{-4}$ s^{-1}). Valid frequencies are indicated with stars; dashed lines are used for clarity and for comparison with figure 3 from Brink (1989).

and $c_{3,1}(2) = f/5$, i.e. waves with more azimuthal modes progress more slowly (for a given p). Analogously, waves with larger radial wavenumbers p are slower as well (for a given n).

3.2. *Flat-topped seamounts or guyots* ($s > 2$)

As mentioned § 1, several tall seamounts are characterized by a flat plateau on the summit. Structures of this kind are well represented by the exponential profile with the shape parameter $s > 2$. Here, some examples for $s = 6$ are presented. Note in figure 1 the pronounced flatness of the summit for this case.

Figure 5(*a–c*) shows the vorticity field of waves $(n, p) = (1, 1)$, $(3, 1)$ and $(6, 1)$. Of course, the azimuthal structure of the waves is similar to the cases shown in the previous subsection: an arrangement of $2n$ counter-rotating cells around the seamount. However, the vorticity cells are strongly confined along the periphery of the circle with radius λ^{-1}: the strength of the waves is nearly zero close to the centre of the seamount and also at large radial distances. The low values over the almost-flat summit are expected since there are weak divergence effects in this region. The confinement of the waves over a narrow region of the guyot periphery is remarkable for the first wave with $n = 1$: note the strong deformation of its dipolar structure in a new-moon fashion in order to be confined within an annular region of radius λ^{-1}.

The rapid decay for large r, on the other hand, is one of the characteristics of the analytical solutions due to the term $\exp(-\lambda^s r^s)$ in the vorticity and velocity fields. For this reason, the structure of waves with larger radial wavenumber p is very similar to the ones presented here, since the amplitudes of successive radial oscillations rapidly decay for large radial distances (as shown in the radial profiles in figure 3).

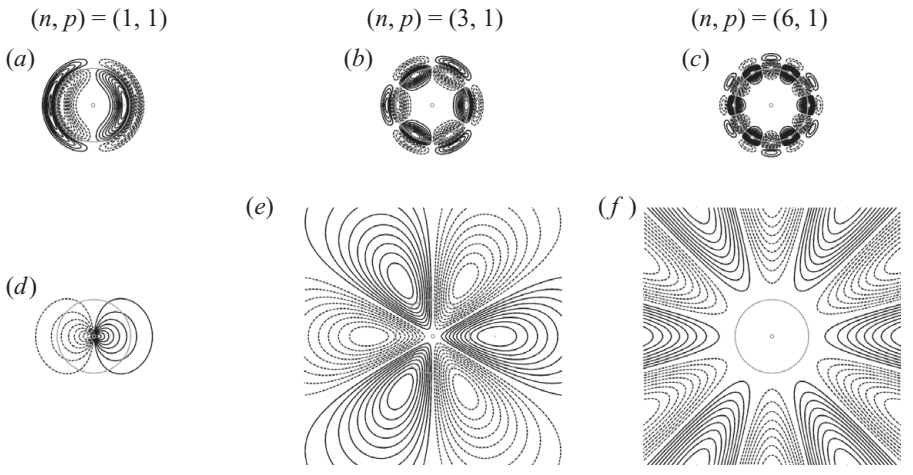

FIGURE 5. Relative vorticity contours of topographic waves. (*a–c*) Over a flat-topped seamount with $s = 6$. (*d–f*) Over a sharp peak seamount with $s = 1$. Contours and grey circle as in figure 2.

The dispersion relation in this example is $\omega/f = n/(6p + n)$, and therefore these waves have a lower frequency compared with those over the less steep seamount presented in the previous subsection. Besides, the corresponding angular speeds, $c_{n,p}(6) = f/(6p + n)$, are slower as well: $c_{1,1}(6) = f/7$, $c_{3,1}(6) = f/9$ and $c_{6,1}(6) = f/12$ (except for $p = 0$).

3.3. *Sharp, conical seamounts* ($s < 2$)

The case of a cone-shaped mountain with $s = 1$ is also shown in figure 1. Figure 5 (*d–f*) presents the corresponding vorticity fields for the same waves $(n, p) = (1, 1)$, (3, 1) and (6, 1). There are strong differences between these cases: the dipolar structure of the first wave is strongly confined within the region around the tip of the seamount. In contrast, the waves with larger azimuthal numbers n are more intense far from the summit and present a triangular configuration of the vorticity cells.

It is also worth noticing that the waves over this sharp seamount have radically different character compared with previous cases over the guyot, as can be seen in figure 5(*a–c*). Another important difference with guyots is that these waves have a greater angular phase speed, $c_{n,p}(1) = f/(p + n)$, compared with those over seamounts with larger s. For these examples, $c_{1,1}(1) = f/2$, $c_{3,1}(1) = f/4$ and $c_{6,1}(1) = f/7$.

Sharp seamounts present a minor restriction on the permitted values of the shape parameter only for the wave with $n = 1$. Although the mathematical solutions of the velocity fields are valid over the entire domain, the vorticity field diverges at $r = 0$ when $n = 1$ and $s < 1$. This can be shown explicitly by calculating the vorticity field and finding that it is proportional to r^{n+s-2}. Thus, for $n = 1$ it is required that $s \geqslant 1$ in order to have a finite vorticity value over the summit. For $n \geqslant 2$ this restriction for s does not exist.

4. Discussion

Exact solutions of barotropic, linear, rigid-lid topographic waves around axisymmetric seamounts have been derived. Even though this type of oscillation has been studied since some time ago, complete analytical expressions for the barotropic

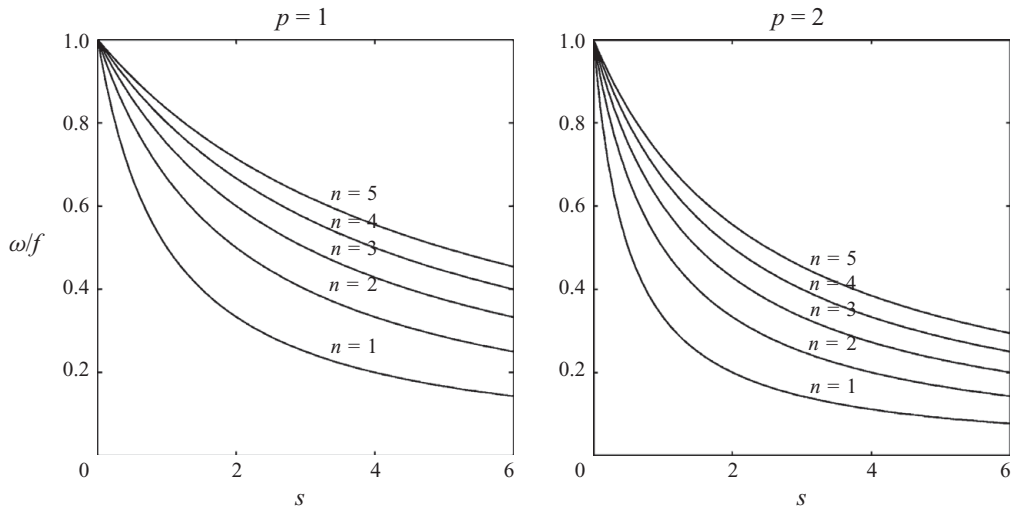

FIGURE 6. Wave frequency as a function of the shape parameter s for different sets of waves.

case have not been reported, as far as the author knows. One of the earlier and more complete works is that of Rhines (1969), who found approximate solutions in terms of Bessel functions over a topography with depth profile proportional to $\exp(r^2)$. (Rhines' paper also considers the coupling of such solutions with an external field dominated by Rossby waves, while in this paper our attention is restricted only to regions over the seamount.) In this study, we report complete solutions of (2.8) in terms of associated Laguerre polynomials, and applied to an infinite set of axisymmetric seamounts with profile proportional to $\exp(r^s)$, with s being a real positive number. Thus, besides the fact that no further approximations are made, the present solutions describe topographic waves over seamounts with very different shapes determined by the parameter s. These topographic features can be flat-topped seamounts for large s (which are frequently observed in the ocean) or sharp peaks for low s (see figure 1).

A number of characteristics of the waves can be noticed from the derived solutions:

(*a*) The main spatial distribution of the waves is essentially given by the azimuthal wavenumber n: the waves are characterized by $2n$ cells of alternating relative vorticity around the summit, and which rotate around the seamount in an anticyclonic direction. Thus, waves with $n = 1$ are formed by a dipolar structure, $n = 2$ by a quadrupole, etc. The radial wavenumber is directly associated with index p, which gives the number of zero crossings of the vorticity radial profiles.

(*b*) The exact dispersion relation has a remarkable simplicity given by expression (2.17). This relation shows the dependence of the wave frequencies on the parameter s, i.e. on the shape of the mountain, as well as on the azimuthal and radial wavenumbers n and p, respectively. For $p \geqslant 1$ the wave frequency increases with n, as shown in figure 4. This behaviour was shown in the nearly barotropic numerical solutions of Brink (1989), who numerically solved the structure of seamount-trapped waves with $s = 2$ (see his figure 3). The frequency of all waves asymptotically tends to f for very large n (fixing p and s). In addition, waves over seamounts with very small s (very sharp peaks) also tend towards the inertial frequency. On the other hand, wave frequencies approach zero for very large p or s. Figure 6 shows the frequency in terms of the shape parameter for different waves.

(*c*) The angular phase speed of waves around the seamount is given by (2.18). This speed approaches zero for large s, p or n. On the contrary, the fastest motion around the seamount, regardless of the shape parameter, is when $(n, p) = (1, 0)$, which completes one turn around the seamount in one inertial period ($c_{1,0}(s) = f$). It is also possible to observe that, for a given pair (n, p), topographic waves over guyots ($s > 2$) tend to have an angular speed slower than waves trapped around a sharp seamount ($s < 2$). In general, the dispersive character of the waves is evident.

(*d*) Over guyots ($s > 2$), the waves are strongly concentrated within an annular region with radius of the order of the topography horizontal scale, λ^{-1}. Wave motions over the summit are nearly zero since flow divergence is very weak over the almost flat top. As mentioned in § 1, this seamount shape is commonly found in the ocean, and therefore the concentration of the wave motion at a distance λ^{-1} from the summit is one of the cases that might have a direct application to oceanographical situations. In contrast, for sharp seamounts ($s < 2$) the waves are strongly concentrated around the peak only when $n = 1$, whilst the vorticity cells have a triangular, spatially extended shape for larger n. There are two remarks of caution about the present model. First, inertial oscillations are obtained for the gravest radial wavenumber $p = 0$ and arbitrary azimuthal wavenumber n, which has not been considered in previous works on topographic trapped waves. In general, other studies deal with subinertial frequencies. Inertial oscillations correspond to the motion of fluid columns unconstrained by pressure forces, but subject to the influence of topographic spatial variations. This can be demonstrated by showing that the solutions (2.21) and (2.22) with $\omega = f$ satisfy the unforced governing equations (2.1)–(2.3) (setting the right-hand sides to zero). This is not very difficult to calculate since the associated Laguerre polynomials are $L_0^{2n/s} = L_0^{2n/s-1} = 1$. The vorticity equation (2.5) and the original equation for the transport function (2.6) are also satisfied. In addition, the group velocity around the seamount is zero for inertial motions: using the dispersion relation (2.17) yields $\partial\omega/\partial n = fsp/(sp + n)^2 = 0$ for $p = 0$; so these oscillations do not transport energy. Actually, they should not be regarded as waves, but as inertial motions in the absence of pressure forces and governed by the presence of the topography. Therefore, in principle, inertial solutions should not be excluded, although their physical meaning must be considered carefully.

Another important point is that the transport function (2.20) diverges for large r. This is a consequence of using the depth profile proportional to $\exp(\lambda^s r^s)$, which obviously also diverges. Therefore, the solutions of ψ are physically unrealistic far from the seamount. In order to avoid this problem, other authors solve the flow over the seamount and then match the solution with an external flow over a flat-bottom ambient ocean. That was the procedure followed by Rhines (1969), who obtained approximate solutions of the radial part of ψ (see (2.8) in § 2). In the present case, in contrast, it has been preferred to obtain exact solutions over the seamount with no further approximations, though it implies paying the price of a transport function increasing indefinitely for $r \gg \lambda^{-1}$. More importantly, the velocity components and the relative vorticity are well-behaved functions on top and around the mountain: they possess values that are physically realistic over these regions, and do not diverge for large distances because they are proportional to $\exp(-\lambda^s r^s)$, which rapidly decays for large r. This is evident from figures 2 and 3, for instance, which show that the main structure of the waves is restricted or trapped around the seamount. As a conclusion, the solutions are physically valid within a range of a few times the length scale of the mountain λ^{-1}.

A more precise estimation of this range in the oceanographical context can be determined by considering that the solutions are valid up to a radial distance D, at which the depth field reaches about 4000 m. Using a 200 m depth at the summit, such a distance is $D = (\ln 20)^{1/s}\lambda^{-1} \approx 3^{1/s}\lambda^{-1}$. Thus, an appropriate criterion depends on the steepness of the seamount. Furthermore, since the velocity and relative vorticity fields have strongly decayed beyond D (due to the term $\exp(-\lambda^s r^s)$), it is reasonable to consider that the solutions are still valid for about three or four times λ^{-1}. This criterion suggests a practical restriction for some solutions over a cone-shaped seamount, since the oscillations are not clearly confined or trapped within a short distance from the top, as in case (6, 1) shown in figure 5(*f*).

Future work will focus on comparing the characteristics of the present wave solutions (e.g. frequencies and angular phase speeds) with seamount-trapped waves described in other observational and numerical studies. According to some authors (e.g. Brink 1989; Chapman 1989; Beckmann & Mohn 2002), predominant waves in oceanographical situations are those with low azimuthal and radial wavenumbers, since frictional effects or bottom roughness would damp higher modes. Thus, the expected manifestation of oceanic waves would be a dipolar structure rotating anticyclonically around a seamount. On the other hand, additional efforts in laboratory experiments are in progress in order to elucidate the nonlinear behaviour of barotropic flows over seamounts, and the signal of linear oscillations; the results will be published elsewhere.

The author gratefully acknowledges the comments of J. L. Ochoa on the earliest version of this paper, and the fruitful remarks made by one of the anonymous referees during the revision process.

Appendix. Recurrence relations for polynomial solutions

The azimuthal velocity component v and the relative vorticity ζ contain one and two r-derivatives of the transport function, respectively, and hence derivatives of the associated Laguerre polynomials. In order to calculate these fields, the following recurrence relation for derivatives of the polynomials is used (Abramowitz & Stegun 1972):

$$\rho\left[L_p^k(\rho)\right]_\rho = pL_p^k(\rho) - (p+k)L_{p-1}^k(\rho), \tag{A 1}$$

which gives

$$\begin{aligned} v = &-\frac{\psi_0\lambda}{h_0}\exp(-\lambda^s r^s)(\lambda r)^{n-1} \\ &\times\left[(sp+n)L_p^{2n/s}(\lambda^s r^s) - (sp+2n)L_{p-1}^{2n/s}(\lambda^s r^s)\right]\cos(\omega t + n\theta), \end{aligned} \tag{A 2}$$

$$\begin{aligned} \zeta = &-\frac{\psi_0\lambda^2}{h_0}\exp(-\lambda^s r^s)(\lambda r)^{n-2} \\ &\times\left\{[(sp+n)(sp+n-s\lambda^s r^s) - n^2]L_p^{2n/s}(\lambda^s r^s)\right. \\ &-[(sp+2n)(2(sp+n) - s(1+\lambda^s r^s)]\,L_{p-1}^{2n/s}(\lambda^s r^s) \\ &\left.+(sp+2n)(sp+2n-s)L_{p-2}^{2n/s}(\lambda^s r^s)\right\}\cos(\omega t + n\theta). \end{aligned} \tag{A 3}$$

Note that polynomials with subindices $p-1$ and $p-2$ appear, which apparently restricts the value of p to be equal to or larger than 2. In order to remove this

limitation, the following recurrence relations are used:

$$L_{p-1}^{k}(\rho) = L_{p}^{k}(\rho) - (p+k)L_{p}^{k-1}(\rho), \tag{A 4}$$

$$L_{p-2}^{k}(\rho) = L_{p}^{k}(\rho) - 2L_{p}^{k-1}(\rho) + L_{p}^{k-2}(\rho). \tag{A 5}$$

For the second expression, it is necessary to use an additional relation for L_p^{k-2} (in order to avoid restrictions on k):

$$(p+k-1)L_{p}^{k-2}(\rho) = (p+1)L_{p+1}^{k-1}(\rho) - (p+1-\rho)L_{p}^{k-1}(\rho). \tag{A 6}$$

The resulting v and ζ fields are given by (2.22) and (2.23). Using appropriate recurrence relations, one can find an infinite way of expressing the solutions. Here we chose those giving the simplest forms.

REFERENCES

Abramowitz, M. & Stegun, I. A. 1972 *Handbook of Mathematical Functions*. National Bureau of Standards.

Arfken, G. 1970 *Mathematical Methods for Physicists*. Academic.

Beckmann, A. & Mohn, C. 2002 The upper ocean circulation at Great Meteor Seamount. Part II: Retention potential of the seamount-induced circulation. *Ocean Dyn.* **52**, 194–204.

Brink, K. H. 1989 The effect of stratification on seamount-trapped waves. *Deep-Sea Res.* **36**, 825–844.

Chapman, D. C. 1989 Enhanced subinertial diurnal tides over isolated topographic features. *Deep-Sea Res.* **36**, 815–824.

Genin, A. 2004 Bio-physical coupling in the formation of zooplankton and fish aggregations over abrupt topographies. *J. Mar. Syst.* **50**, 3–20.

Gill, A. E. 1982 *Atmosphere-Ocean Dynamics*. Academic.

Haidvogel, D. B., Beckmann, A., Chapman, D. C. & Lin, R. Q. 1993 Numerical simulation of flow around a tall isolated seamount. Part II: Resonant generation of trapped waves. *J. Phys. Oceanogr.* **23**, 2373–2391.

Hillier, J. K. & Watts, A. B. 2007 Global distribution of seamounts from ship-track bathymetry data. *Geophys. Res. Lett.* **34**, L13304.

Huppert, H. E. & Bryan, K. 1976 Topographically generated eddies. *Deep-Sea Res.* **23**, 655–679.

Huthnance, J. M. 1974 On the diurnal tide currents over Rockall Bank. *Deep-Sea Res.* **21**, 23–35.

Nycander, J. & Lacasce, J. H. 2004 Stable and unstable vortices attached to seamounts. *J. Fluid Mech.* **507**, 71–94.

Rhines, P. B. 1969 Slow oscillations in an ocean of varying depth. Part 2. Islands and seamounts. *J. Fluid Mech.* **37**, 191–205.